THE JOURNAL OF BIOLOGICAL CHEMISTRY VOL. 286, NO. 19, pp. 17351–17358, May 13, 2011

Structural Basis for Ligand Recognition and Discrimination of a Quorum-quenching Antibody*

Received for publication, February 17, 2011, and in revised form, March 13, 2011 Published, JBC Papers in Press, March 23, 2011, DOI 10.1074/jbc.M111.231258

Robert N. Kirchdoerfer[‡], Amanda L. Garner[§], Caralyn E. Flack[¶], Jenny M. Mee[§], Alexander R. Horswill[¶], Kim D. Janda[§‖], Gunnar F. Kaufmann[§1], and Ian A. Wilson[‡‖2]**

*From the Departments of [‡]Molecular Biology and [§]Chemistry and Immunology & Microbial Science, [‖]The Skaggs Institute for Chemical Biology, **Worm Institute for Research and Medicine, The Scripps Research Institute, La Jolla, California 92037 and the [¶]Department of Microbiology, University of Iowa, Iowa City, Iowa 52242*

In the postantibiotic era, available treatment options for severe bacterial infections caused by methicillin-resistant *Staphylococcus aureus* have become limited. Therefore, new and innovative approaches are needed to combat such life-threatening infections. Virulence factor expression in *S. aureus* is regulated in a cell density-dependent manner using "quorum sensing," which involves generation and secretion of autoinducing peptides (AIPs) into the surrounding environment to activate a bacterial sensor kinase at a particular threshold concentration. Mouse monoclonal antibody AP4-24H11 was shown previously to blunt quorum sensing-mediated changes in gene expression *in vitro* and protect mice from a lethal dose of *S. aureus* by sequestering the AIP signal. We have elucidated the crystal structure of the AP4-24H11 Fab in complex with AIP-4 at 2.5 Å resolution to determine its mechanism of ligand recognition. A key Glu^{H95} provides much of the binding specificity through formation of hydrogen bonds with each of the four amide nitrogens in the AIP-4 macrocyclic ring. Importantly, these structural data give clues as to the interactions between the cognate staphylococcal AIP receptors AgrC and the AIPs, as AP4-24H11·AIP-4 binding recapitulates features that have been proposed for AgrC-AIP recognition. Additionally, these structural insights may enable the engineering of AIP cross-reactive antibodies or quorum quenching vaccines for use in active or passive immunotherapy for prevention or treatment of *S. aureus* infections.

Prokaryotic and eukaryotic single-cell organisms use cell-to-cell communication to coordinate their gene expression as they adapt to changing environmental conditions and compete with multicellular organisms. This chemical exchange of information among microorganisms has been termed "quorum sensing" (QS)[3] (1, 2). With the emergence of highly antibiotic-resistant bacterial strains, including methicillin-resistant *Staphylococcus aureus*, new approaches for combating microbial infections are needed desperately (3–5). Although most antibiotics target essential metabolic pathways, inhibition of virulence-associated processes, such as QS signaling, attenuates the bacteria without exerting as much selective pressure, thereby decreasing development of resistance. Thus, this approach represents a new and innovative concept for antimicrobial drug discovery and might hold promise for the design of the elusive *S. aureus* vaccine (6–9).

The *agr* (accessory gene regulator) QS system in *S. aureus* contributes to pathogenesis by orchestrating the temporal cell density-dependent expression of virulence genes. During exponential growth, the bacterial cell surface and adhesion molecules are expressed, whereas upon entering stationary phase, the expression pattern changes and results in the down-regulation of surface proteins and activation of genes encoding exoproteins and toxins (10–12). The *agr* locus is composed of two transcriptional units: the *agr* (or P2) operon under control of the P2 promoter and RNAIII, the *de facto* effector of *agr* QS, regulated by the P3 promoter (see Fig. 1*A*) (13, 14). The P2 operon consists of four genes, *agrBDCA*, which encode the proteins responsible for the synthesis of and response to the QS peptides. The *agrD* gene encodes a 46-amino acid AIP precursor peptide that is processed and cyclized by SpsB and AgrB (15) via formation of a thiolactone bond between a cysteine and the carboxyl group of the C-terminal residue. The resulting AIP is then secreted into the extracellular environment (16). The cognate receptor for the AIPs is the transmembrane sensor kinase AgrC. The N-terminal receptor domain of AgrC is predicted to consist of six membrane-spanning helices with three extracellular loops that constitute the AIP binding site (17–19). Upon AIP binding, the C-terminal cytoplasmic kinase domain relays the signal to AgrA and phosphorylated AgrA binds to the P2 and P3 promoters to activate AIP-controlled gene expression (20). Interestingly, *S. aureus* strains can be divided into four distinct *agr* subgroups, generally referred to as groups I, II, III, and IV. In each *agr* group, the AgrC receptor recognizes a specific AIP struc-

* This work was supported in part by National Institutes of Health Grants AI078921 (to A. R. H.), AI080715 (to G. F. K.), and AI042266 and CA058896 (to I. A. W.). This work was also supported by The Skaggs Institute (to I. A. W. and K. D. J.). The Advanced Photon Source at Argonne National Laboratory is supported by the U. S. Department of Energy, Office of Science, Office of Basic Energy Sciences Contract DE-AC02-06CH11357. This is Paper 20569 from The Scripps Research Institute.

The atomic coordinates and structure factors (codes 3QG6 and 3QG7) have been deposited in the Protein Data Bank, Research Collaboratory for Structural Bioinformatics, Rutgers University, New Brunswick, NJ (http://www.rcsb.org/).

[1] To whom correspondence may be addressed: 10550 N. Torrey Pines Rd., BCC578, La Jolla, CA 92037. Tel.: 858-784-2517; Fax: 858-784-2595; E-mail: kaufmann@scripps.edu.

[2] To whom correspondence may be addressed: 10550 N. Torrey Pines Rd., BCC206, La Jolla, CA 92037. Tel.: 858-784-9706; Fax: 858-784-2980; E-mail: wilson@scripps.edu.

[3] The abbreviations used are: QS, quorum sensing; AIP, autoinducing peptide; CDR, complementarity determining region.

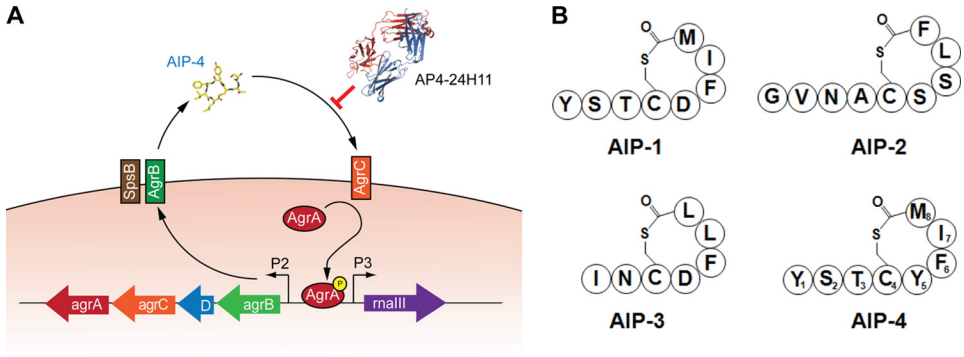

FIGURE 1. **The *agr* operon.** *A*, the *agrBDCA* genes encode the AgrB, AgrD, AgrC, and AgrA proteins, which are all involved in the biosynthesis of AIPs. The propeptide AgrD is processed by AgrB and SpsB into AIP-4, which is sensed by the two-component regulatory system AgrC and AgrA. Phosphorylated AgrA activates transcription at the P2 and P3 promoters. Autoinduction of the *agr* operon leads to induction the response regulator, RNA III, and changes in gene expression. AP4–24H11 sequesters AIP-4 and prevents the activation of AgrC. *B*, schematic representation of the four AIPs encoded by *agr* groups I–IV. The residues of AIP-4 are numbered to illustrate and clarify the nomenclature.

ture (*i.e.* AIP-1 through AIP-4, Fig. 1*B*) that promotes RNAIII transcription. Through so-called "bacterial interference," the AIP signal of one *agr* group can compete for the AgrC receptor of another group and inhibit RNAIII transcription (21). Based on these observations, the AIPs are often classified into three cross-inhibitory groups: (i) AIP-1 and AIP-4, (ii) AIP-2, and (iii) AIP-3. AIP-1 and AIP-4 are grouped together because these structures differ by only one amino acid (Asp^5 or Tyr^5, respectively) (17, 19).

Recently, blockade of quorum sensing has been shown to attenuate the expression of virulence factors in Gram-positive bacteria (22–24). Park *et al.* (24) reported the generation of the murine monoclonal antibody AP4-24H11 that sequesters AIP-4 utilized by *S. aureus agr* group IV strains as a QS signaling molecule. Treatment of *S. aureus* cultures with AP4-24H11 caused an increase in protein A expression and decreases in α-hemolysin expression and RNA III transcription, consistent with suppression of QS signaling (24). Most impressive, however, was the ability of this antibody to protect mice from *S. aureus* infections *in vivo*, including abscess formation in a skin infection model and lethality in a peritonitis model using a *S. aureus* group IV strain.

Here, we present the structure of the AP4-24H11 Fab in complex with AIP-4, which is the first structure of a quorum-sensing peptide bound to a receptor protein, in this case, an antibody. These structural data provide some possible insights into the interactions between the cognate staphylococcal AIP receptors AgrC and the AIPs, as the antibody binding to AIP-4 shares many features that have been hypothesized for recognition of AIP by AgrC.

EXPERIMENTAL PROCEDURES

Fab Production, Sequencing, and Purification—IgG was produced (25) and sequenced (26) using established methods. N-terminal sequencing of the AP4-24H11 heavy and light protein chains was performed at The University of Texas Biomedical Branch, Biomolecular Resource Facility. AP4-24H11 IgG was digested to Fab and Fc using 4% (w/w) papain for 4 h (27). The Fab was purified by successive protein A and protein G chromatography. Fab was further purified by MonoS where the Fab eluted at concentrations of 220–240 mM sodium chloride. The purified protein was concentrated to 19 mg/ml in 100 mM sodium acetate (pH 5.5), 1.25 mM EDTA, and 0.02% (w/v) sodium azide.

Crystallization and Data Collection—The AP4-24H11 Fab alone was crystallized by vapor diffusion using 1.0-μl sitting drops. Drops contained equal volumes (0.5 μl) of purified protein and the precipitant (20% PEG 4000, 0.2 M diammonium hydrogen phosphate (pH 8.0)). Crystals appeared after 1 month and grew as clusters of needles. The diffraction data were indexed in space group H3 with one molecule in the asymmetric unit.

AIP-4 was synthesized as described previously (24). AIP-4 at a final concentration of 5 mM was mixed with the AP4-24H11 Fab (13-fold excess of AIP-4 to Fab) immediately before setting up for crystallization by vapor diffusion using 1.0 μl sitting drops. The AIP-4·AP4-24H11 Fab complex was co-crystallized using equal volumes (0.5 μl) of the protein·ligand complex and precipitant (29 mM zinc acetate, 20% PEG 4000, 100 mM sodium cacodylate (pH 6.5)). Crystals appeared after 1 day and grew as clusters of long needles or plates and were cryoprotected in 20% glycerol prior to flash freezing in liquid nitrogen. The crystals were highly anisotropic with almost no diffraction observable when the beam was parallel to the plane of the very thin, plate-like crystals. The data were indexed in monoclinic space group $P2_1$ with two Fab molecules in the asymmetric unit. All data were collected at the Advanced Photon Source beamline 23ID-B (Argonne National Laboratory) and were processed with HKL2000 (28).

Structure Determination, Refinement, and Analysis—The AP4-24H11 Fab structure was solved by molecular replacement using Phaser (29). Domains of Protein Data Bank code 15C8 (30) were used as a search model based on homology to the AP4-24H11 Fab framework regions. Coot (31) was used for model building, and Refmac (32) was used for refinement. Only Leu^{L51} and Pro^{H149} are designated as Ramachandran "outliers," but both have a good fit to the corresponding electron density. Leu^{L51} is in a γ-turn commonly found in almost all Fab structures (33). Additional density in the binding site was modeled as 10 atoms of PEG. There was weak or missing $2F_o - F_c$ density for heavy chain residues 128–130, 133, and 134, that is also

absent or weak in many other Fab structures, and these residues were omitted from the refined structure.

The AIP-4·AP4-24H11 Fab complex structure was determined by molecular replacement using the AP4-24H11 Fab solution. The AIP-4 ligand was initially built using Coot. AIP-4 geometric restraints were created with the PRODRG online server (34) and Sketcher (35). No density in $2F_o - F_c$ maps at the 1.0σ level could be seen for AIP-4 Tyr^1, and this residue was omitted from the model. Coot was used for model building, and Buster-TNT (36) was used for refinement. Final rounds of refinement were performed in Refmac. Five zinc ions in the asymmetric unit mediate contacts between Fab molecules and aid in crystal packing interactions. Weak or missing $2F_o - F_c$ map density was again noted for heavy chain residues 129, 130, 133, and 134, and these residues were omitted from the structure.

Both Fab structures were numbered in the Kabat convention using the Abnum online server (37) and Pdbset (35). MolProbity (38) was used to calculate Ramachandran statistics. The 24H11-AIP-4 Fab structure was analyzed using Contacsym and MS (39, 40) to calculate buried surface area and enumerate van der Waals interactions. HBPLUS (41) was used to identify hydrogen bonds between AIP-4 and AP4-24H11. One of the Fab complexes (Fab chains A (light chain) and B (heavy chain) and AIP-4 chain D) was used for all calculations and measurements reported here.

Assessing Quorum Quenching Using S. aureus YFP Reporter Strains—Plasmid pDB59 (42) was transformed into four *S. aureus* strains representing *agr* group I (USA300 LAC), *agr* group II (SA502A), *agr* group III (MW2), and *agr* group IV (MN EV). All *S. aureus* reporter strains were grown overnight in tryptic soy broth supplemented with chloramphenicol at 10 μg/ml at 37 °C with shaking. For antibody inhibition testing, cultures were diluted 100-fold into fresh media, incubated for 1 h at 37 °C, and 180 μl was dispensed into wells of a microtiter plate (Costar 3603). AP4-24H11 was diluted to a working concentration of 2 mg/ml in PBS, and 2-fold serial dilutions were generated in PBS to a final concentration of 9.8×10^{-4} mg/ml. 20 μl of each antibody dilution was added to the reporter cultures in the microtiter plates in quadruplicate, resulting in an additional 10-fold dilution. As controls, PBS was used as a mock sample (no antibody), and an unrelated mouse IgG2a isotype control antibody was added at 2 mg/ml. The filtered spent medium containing AIP-1 from LAC or AIP-3 from MW2 was used as inhibition controls. Plates were incubated for 24 h at 37 °C with shaking at 200 rpm. Absorbance and fluorescence was measured in a Tecan Infinite M200 plate reader using an excitation wavelength of 485 nm and an emission wavelength of 530 nm.

RESULTS

Park *et al.* (24) demonstrated that AP4-24H11 cross-reacts with AIP-1 and AIP-4, resulting in the complete suppression of QS-regulated virulence factor α-hemolysin expression in an *agr* IV *S. aureus* strain and partial inhibition in a group I isolate. To clearly delineate the extent of AIP cross-reactivity of AP4-24H11, four *S. aureus* reporter strains with the *agr* P3 promoter driving expression of YFP were constructed to represent each *agr* group. A range of AP4-24H11 concentrations was mixed with early growth phase cultures to assess antibody impact on actively growing *S. aureus* (Fig. 2). Notably, co-incubation of AP4-24H11 with *S. aureus* reporter strains belonging to *agr* group IV (IC_{50} = 0.00011 mg/ml [0.73 nM]) and to a lesser extent group I (IC_{50} = 0.040 mg/ml [27 nM]) resulted in significant decreases in YFP production in a dose-dependent manner, whereas QS signaling in *agr* groups II and III strains was not affected significantly by the antibody (IC_{50} >1 μM; Fig. 2). These data demonstrate that AP4-24H11 is greater than 350 times more potent in quenching *agr* signaling in a cognate group IV strain than in an *S. aureus* group I isolate that produces the nearly sequence-identical AIP-1.

To elucidate the molecular interactions that allow for antibody discrimination between similar quorum-sensing peptides, we determined the crystal structure of the AIP-4·AP4-24H11 Fab complex at 2.5 Å resolution (Table 1). Although electron density in $2F_o - F_c$ maps (contoured at 1.0σ) for the thiolactone ring of AIP-4 is well defined, the three residue N-terminal tail generally is less ordered. However, in one of the two Fab copies in the asymmetric unit, electron density was present for AIP-4 Ser^2 and Thr^3. The peptide bonds in the thiolactone ring are oriented such that most of the backbone carbonyl oxygens point in the general direction of the light chain, and the amide nitrogens are oriented toward the heavy chain. The side chains of the AIP-4 residues splay outwards from the ring.

The AIP-4 macrocycle is intercalated into the antibody combining site (Fig. 3). This disposition directs the AIP-4 Phe^6, Ile^7, and Met^8 side chains into the binding site and accounts for the majority of its buried surface area (Table 2). The AIP-4 ligand is recognized by AP4-24H11 primarily through the heavy chain (60%) (Table 3), although all complementarity determining regions (CDRs) make contributions, as well as some framework regions (4.8%). Although CDR1 of the heavy chain (CDRH1) buries the most ligand surface area of any CDR, the most striking features with respect to ligand recognition involve CDRH3.

Despite its short length of only four residues, the CDRH3 loop is responsible for a large portion of the ligand buried surface area, which primarily results from a glutamic acid (Glu^{H95}; according to Kabat numbering (37)) that is positioned at the apex of the loop. The Glu^{H95} carboxyl is oriented toward the center of the AIP-4 thiolactone ring and hydrogen bonds with each of the four amide nitrogens in the ring (Fig. 4). Additionally, the aliphatic portion of the Glu^{H95} side chain runs parallel to the AIP-4 Met^8 contributing to the burial of hydrophobic surface area. Thus, Glu^{H95} accounts for 13.1% of the total ligand buried surface, greater than twice that of any other single residue.

During model building and refinement, we observed strong, spherical density at a distance of 4–5 Å from three of the AIP-4 main chain carbonyl oxygens. Furthermore, many oxygen-containing groups in the nearby light chain are oriented in the direction of this unaccounted for density. Additionally, the plane of the aromatic ring of Tyr^{L32} is oriented such that the ζ-carbon is centered 4.5 Å from the center of this site (43, 44). These data suggest the presence of a monovalent cation that forms a cation-π interaction with Tyr^{L32}, as well as electrostatic interactions with neighboring electron-donating

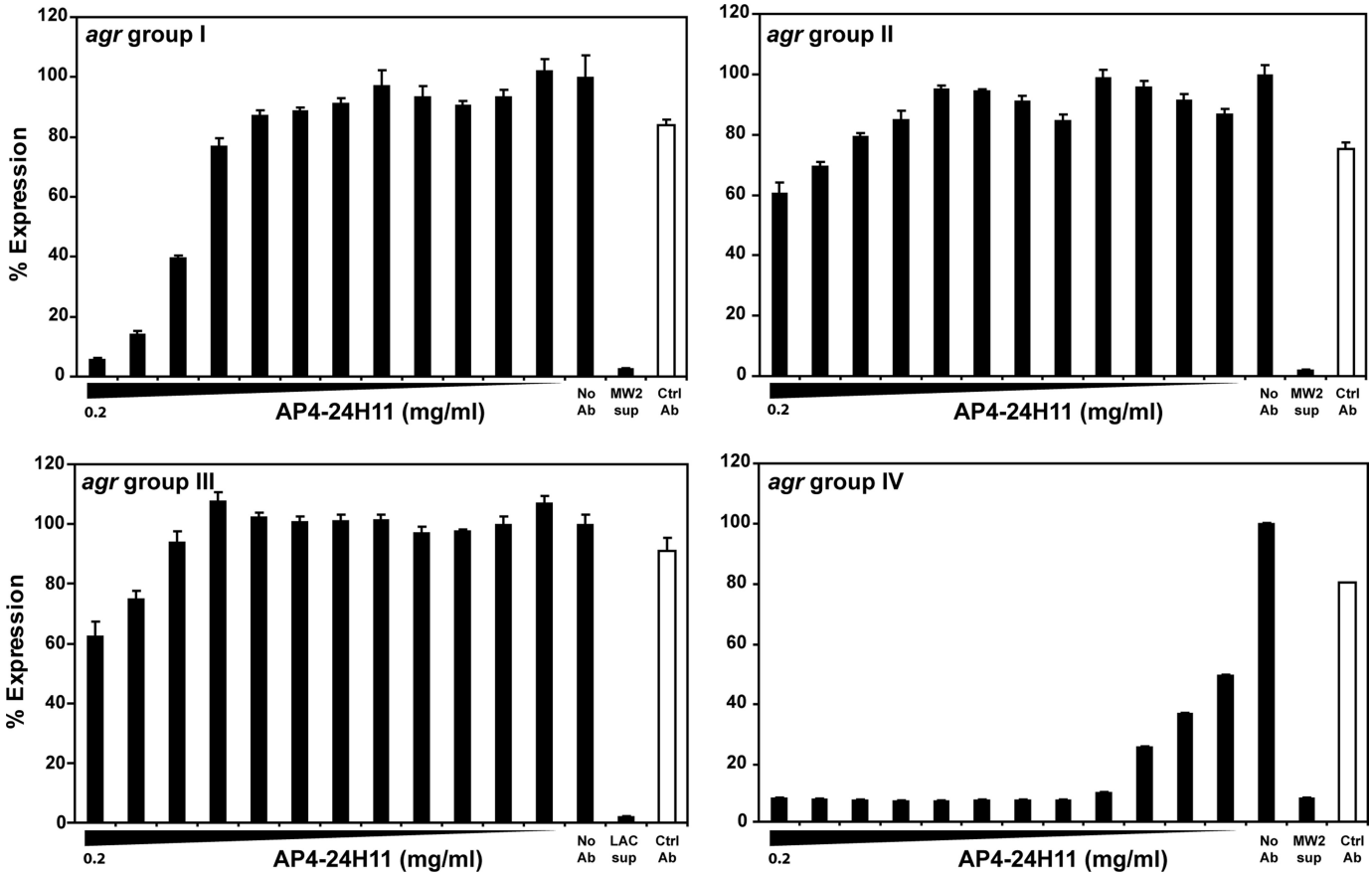

FIGURE 2. **High *agr* specificity of quorum-sensing signaling inhibition mediated by AP4-24H11 in *S. aureus*.** *S. aureus* strains containing a plasmid with an *agr* P3-YFP promoter fusion (pDB59) were used to examine the quorum-quenching activity of AP4-24H11. Reporter strains representing each of the four *agr* groups were constructed and incubated with AP4-24H11 in concentrations ranging from 0.2 to 9.8 $\times$ 10^{-5} mg/ml. As controls (*Ctrl*), assays containing no antibody or an isotype control antibody (0.2 mg/ml) were included. For *agr* inhibition controls, supernatants (*sup*) from MW2 containing AIP-3 or LAC containing AIP-1 were included as indicated. Using AP4-24H11, strong inhibition of *agr* group IV and modest inhibition of *agr* group I was observed, whereas minimal inhibition of *agr* group II and III was evident only at high AP4-24H11 doses. *Error bars* represent S.D. of quadruplicate samples, and each experiment was repeated.

groups. We have, therefore, modeled this additional density as a monovalent sodium cation. Subsequent refinement showed that it has similar B-values to the side chain of Tyr^{L32} and provides some validation for this assignment. Nevertheless, although we cannot be absolutely certain of the identity of this presumed ion, the positive charge of the sodium would provide stabilizing interactions with the carbonyl oxygens of the thiolactone ring. This interaction, together with the Glu^{H95} hydrogen bonding to the amide nitrogens of the macrocycle, would facilitate antibody recognition of both faces of the AIP-4 ring.

Thus far, we have described the AIP-4-AP4-24H11 interaction and specificity as resulting from burial of the C-terminal hydrophobic side chains, recognition of the AIP-4 peptide backbone by hydrogen bonding to Glu^{H95} and proposed electrostatic interactions with a metal ion. However, Park *et al.* (24), as well as the *S. aureus* reporter assay data (Fig. 2), demonstrated that AP4-24H11 is able to discriminate finely between the AIP molecules of different *S. aureus* groups. In fact, AIP-1 and AIP-4 differ only at position 5 where AIP-1 contains an aspartic acid rather than tyrosine in AIP-4 (Fig. 1*B*), which might account for the reduced inhibition of toxin production (24) and YFP expression in the reporter assay (Fig. 2*A*) in an *agr* group I strain by AP4-24H11. Structurally, AIP-4 Tyr^5 makes a CH-π bond with Tyr^{H33} where one of the AIP-4 Tyr^5 ϵ-carbons is positioned 3.5–4.0 Å from the Tyr^{H33} aromatic ring (Fig. 5*A*). Similarly, AIP-4 Phe^6 makes a CH-π bond with Tyr^{L49} with its ζ-carbon positioned 4.1–4.5Å from the Tyr^{L49} aromatic ring (Fig. 5*B*). These are the only interactions where the AIP-4 side chains are recognized specifically by the antibody and may account for the observed discrimination of AIP-1 and AIP-4 by AP4-24H11. Although CH-π, or edge-to-face, interactions are typically regarded as weak, they can contribute 0.6–1.3 kcal/mol in stabilization energy (45, 46). Thus, although recognition of the main chain conformation and burial of hydrophobic surfaces in AIP-4 likely are the major modes of interaction with AP4-24H11, these additional aromatic-aromatic interactions aid in the specificity of ligand recognition. For AIP-2 and AIP-3, although AIP-4 Ile^7 does not engage in any specific interactions, the Leu^7 side chain in other AIPs might create steric clashes within the binding site (Fig. 5*B*). Additionally, the long unbranched AIP-4 Met^8 packs parallel to the Glu^{H95} side chain and part of the main chain, in contrast to the branched side chains of the other AIPs at this position which would likely have steric clashes with the Fab in this region (Fig. 5*C*).

To gain additional insight into the structural dynamics of the AIP-4-AP4-24H11 interactions, we also determined the struc-

TABLE 1
Data collection and refinement statistics

	AIP-4·AP4–24H11	AP4–24H11·PEG
Data collection		
Wavelength (Å)	0.980	1.033
Resolution (Å)	2.50 (2.50-2.59)[a]	2.80 (2.80-2.90)
Space group	$P2_1$	H3
Cell dimensions	$a = 68.4$, $b = 98.5$, $c = 73.7$ Å; $\alpha = 90$, $\beta = 114.0$, $\gamma = 90°$	$a = 183.2$, $b = 183.2$, $c = 42.6$ Å; $\alpha = 90$, $\beta = 90$, $\gamma = 120°$
No. of observations	83,591	29,584
Unique reflections	29,017	13,033
Redundancy	2.9 (2.4)[a]	2.3 (2.1)
Completeness (%)	94.3 (90.7)	97.9 (94.0)
R_{sym} (%)[b]	16.8 (43.1)	10.8 (40.8)
I/σ	6.4 (1.6)	7.7 (1.9)
Refinement statistics		
Resolution	39.7-2.50 (2.57-2.50)	90-2.78 (2.85-2.78)
No. of reflections (working)	25,883	11,734
No. of reflections (test)	1,477	644
R_{cryst} (%)[c]	18.3 (26.4)	19.5 (29.2)
R_{free} (%)[d]	23.8 (34.0)	24.0 (36.3)
No. of moles in asu[g]	2	1
No. of Fab atoms	6,586	3,272
No. of ligand atoms	110 (AIP4)	27 (PEG)
No. of water molecules	294	51
No. of metal ions	11	1
Overall B values (Å^2)		
Antibody	27.1	53.5
Ligands	26.6 (AIP4)	59.5 (PEG)
Water	19.8	38.4
Ions	31.1/50.5 (Na^{+1}/Zn^{+2})	53.4 (Na^{+1})
Wilson B-value (Å^2)	40.6	41.2
Ramachandran plot (%)[e]		
Favored	96.9	93.1
Allowed	3.1	6.4
Disallowed	0.0	0.5
r.m.s.d.[f]		
Bond length (Å)	0.010	0.008
Angle	1.46°	1.21°

[a] Outer shell.
[b] $R_{sym} = \Sigma_{hkl}|I - \langle I\rangle|/\Sigma_{hkl}|I|$.
[c] $R_{cryst} = \Sigma_{hkl}|F_{obs} - F_{calc}|/\Sigma_{hkl}F_{obs}$.
[d] R_{free} is the same as R_{cryst} except for 5% of the data excluded from refinement.
[e] Ramachandran statistics were calculated with MolProbity (39).
[f] r.m.s.d., root mean square deviation.
[g] asu, asymmetric unit.

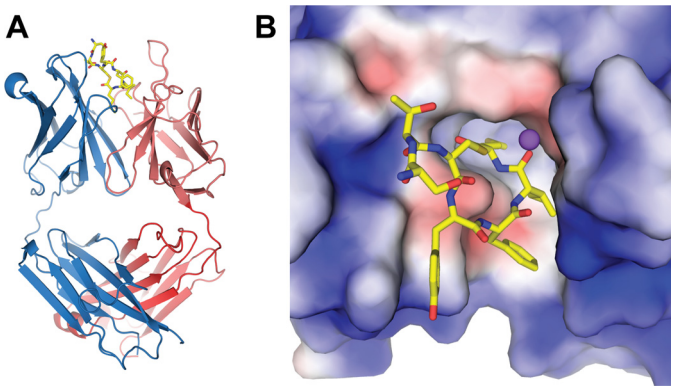

FIGURE 3. **Crystal structure of AIP-4·AP4-24H11.** *A*, structure of AP4-24H11 Fab with AIP-4 inserted between the heavy chain (*blue*) and light chain (*red*) in the combining site. *B*, electrostatic surface of the 24H11 binding site (+3.0 kV (*blue*) to −3.0 kV (*red*)). The hydrophobic residues AIP-4 Phe^6, Ile^7, and Met^8 are buried in a hydrophobic pocket. The negative potential beneath the ring arises from Glu^{H95}. A sodium ion is modeled as a *purple sphere*.

TABLE 2
AIP-4 contacts with AP4-24H11

AIP-4 Residue	Main chain[a]	Side chain[a]	Buried surface (Å^2)
Ser^2	0/0	0/0	14.5
Thr^3	1/4	0/6	56.6
Cys^4	0/2	0/4	22.1
Tyr^5	1/3	0/23	72.6
Phe^6	1/5	0/9	98.1
Ile^7	2/4	0/13	88.7
Met^8	1/17	0/20	122.3
Total	6/35	0/65	474.9

[a] Hydrogen bonds/van der Waals contacts.

TABLE 3
Contribution of AP4-24H11 regions to AIP-4 buried surface
Regions were defined using the contact numbering scheme (37).

Region	Buried surface contribution (%)
CDRL1	10.5
CDRL2	14.4
CDRL3	12.7
FRL4	2.2
FRH1	0.2
CDRH1	21.6
FRH2	2.4
CDRH2	17.1
CDRH3	18.7

ture of the AP4-24H11 Fab alone (2.8 Å resolution) to identify any changes that might take place upon antigen binding (Table 1). It is important to note that this AP4-24H11 Fab structure is not truly an apo-Fab structure. Extra density at the bottom of the antibody-combining site was modeled as PEG, which was present in the crystallization solution. This finding is reminiscent of the crystal structure of the quorum quenching antibody RS2–1G9, an anti-acyl homoserine lactone mAb, solved previously by our laboratory that also harbored an ethylene glycol

molecule in the absence of the natural acyl homoserine lactone ligand (47). The PEG molecule occupies the location that is normally filled by the AIP-4 Ile^{7} and AIP-4 Met^{8} side chains. Superimposition of the variable regions revealed that, although no major rearrangements or loop movements occur upon ligand binding, the heavy chain shows small, but important, conformational changes in the CDR loops in the absence of AIP-4. The largest changes are observed in CDRH1 and CDRH3. In CDRH1, Tyr^{H33} reorients to form one of the CH-π interactions with AIP-4 Tyr^{5}. Interestingly, this reorientation also allows Tyr^{H33} to form a cation-π interaction with Arg^{H94}. These changes in CDRH1 also rotate and reposition Asn^{H32} to avoid a steric clash with AIP-4. In CDRH3, the backbone torsional angles of Glu^{H95} also change to avoid a clash with AIP-4 and enable it to pack parallel to the AIP-4 Met^{8} side chain. In CDRH2, a tyrosine side chain has to change its rotamer to avoid a clash upon AIP-4 binding. On the other hand, the light chain shows almost no structural change induced by ligand binding, even at the side chain level. Notably, we again found spherical density positioned above Tyr^{L32} implying that the proposed monovalent cation is prebound to the antibody.

DISCUSSION

Crystal structures of AP4-24H11 have revealed how the antibody interacts with the AIP-4 peptide, the QS signaling molecule of *S. aureus agr* group IV. Recognition of AIP-4 by AP4-24H11 is accomplished primarily through polar contacts with the AIP-4 macrocyclic peptide backbone and nonpolar interactions with the side chains of the C-terminal hydrophobic residues. Glu^{H95} is a key residue as it contributes four of the six hydrogen bonds from the antibody to AIP-4 and thus buries a large portion of the AIP-4 hydrophobic surface area. These hydrogen bonds specifically recognize the macrocyclic configuration of the AIP-4 backbone. Analysis of the Fab structures clearly reveals how AP4-24H11 can discriminate among the different AIP molecules. We hypothesize that AIP-1 Asp^{5} would be unable to participate in the same CH-π interaction with the mAb as the corresponding AIP-4 Tyr^{5}, thus conferring the ability to discriminate between AIP-1 and AIP-4. With regard to AIP-2 and -3, each has a leucine in lieu of AIP-4 Ile^{7} and a phenyalanine and a leucine, respectively, in place of AIP-4 Met^{8}, none of which can be accommodated as well as the AIP-4 residues.

It seems prudent to compare this structural information on the interactions of AIP-4 and AP4-24H11 with those proposed for AgrC, the native *S. aureus* AIP receptor, and, in particular, with AgrC from group IV. Novick and co-workers (48) hypothesized that positions 7 and 8 of the AIPs need to be nonpolar, which led to the hypothesis that AgrC buries these residues in a hydrophobic pocket. Also, the requirement of a specificity-determining interaction, *e.g.* AIP-1 Asp^{5} and AIP-4 Tyr^{5}, was proposed (48). Lastly, it has been demonstrated the N-terminal AIP tail is essential for receptor activation and signaling of AgrC (22). Remarkably, the first two of these three postulated key features are recapitulated in the antibody recognition and binding to AIP-4, namely the energetically favorable burial of hydrophobic AIP-4 residues and discrimination between AIP-4 Tyr^{5} and AIP-1 Asp^{5}. However, the tail region of AIP-4 makes only limited contact with AP4-24H11. The hallmark feature of AP4-24H11, *i.e.* the prominent role of Glu^{H95}, might even be reflected in the AgrC receptors of all groups, as the extracellular loops contain several candidate acidic residues.

Notably, AP4-24H11 recapitulates the recognition patterns of group IV AgrC, in that the native receptor recognizes and is activated by AIP-4, and to a lesser extent by AIP-1 (19). Recently, Novick and colleagues detailed the evolution of *agr* genes, proposing *agr* groups I and II diverged from a common ancestor early on, and groups III and IV split from group I more

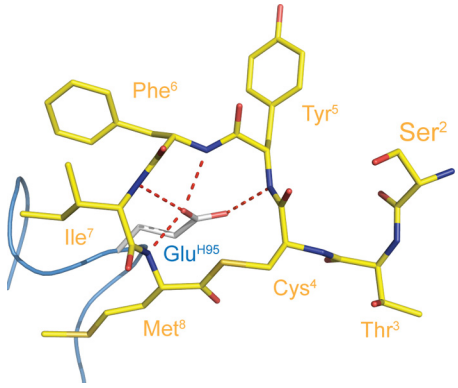

FIGURE 4. **Antibody recognition of the AIP-4 main chain conformation.** Glu^{H95} in CDRH3 extends toward the center of the AIP-4 macrocyclic ring. The Glu^{H95} side chain makes hydrogen bonds to each of the amide nitrogens of AIP-4 residues 5–8.

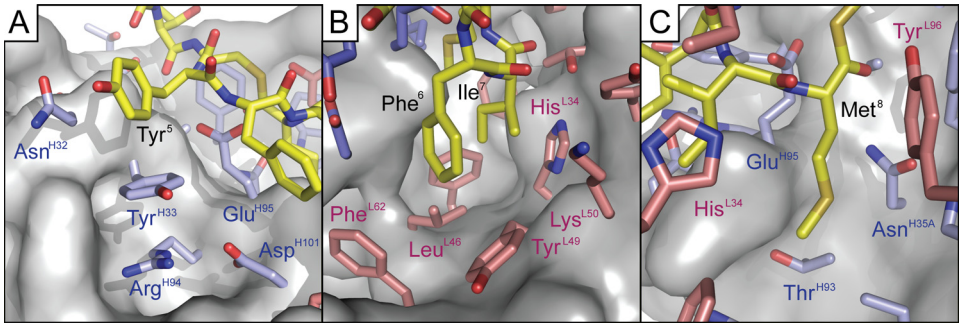

FIGURE 5. **Molecular interactions between AP4-24H11 and AIP-4 side chains.** Close-up illustration of the interactions of AIP-4 macrocycle side chains with the antibody combining site of AP4-24H11. *A*, the aromatic ring of AIP-4 Tyr^{5} is positioned 3.5–4.0Å from Tyr^{H33}, creating a CH-π bond. *B*, Phe^{6} of AIP-4 makes a CH-π bond with Tyr^{L49} with the ζ-carbon of AIP-4 Phe^{6} positioned 4.1–4.5Å from the Tyr^{L49} aromatic ring. Ile^{7} does not engage in any specific interactions, but the leucine side chain found in other AIPs might create steric clashes within the binding site. *C*, Met^{8} of AIP-4 packs along the Glu^{H95} side chain and part of the main chain, which might prevent interactions with the branched side chains found in other AIPs at this position.

recently. In fact, the *agr* group IV appears to be the most recent evolution of an *agr* group (49). In this context, it is important to note that evolution affecting *agr* diversification absolutely requires the coordination of mutations within all three key genes encoding *agr* group specificity, namely the pro-AIP (AgrD), the AIP receptor (AgrC) and the pro-AIP processing enzyme (AgrB), thus severely restricting the possible mutational space. However, this mutational restriction might explain the somewhat relaxed ligand specificity as cross-recognition of an existing AIP, as well as a newly evolved AIP, would most likely be a key intermediate step in the evolution of new *agr* groups (49). The antibody structure then might provide hints for how group IV AgrC is able to still maintain AIP-1 recognition while developing a strong preference for AIP-4.

The structures reported here also suggest how to engineer AP4-24H11 for new or enhanced recognition of the other known AIP molecules for broad spectrum neutralization. For example, directed mutagenesis of the region responsible for the AIP-4 Tyr^5 and AIP-1 Asp^5 discrimination might switch the antibody preference from AIP-4 to AIP-1. Alternatively, modification of the antibody combining site to more readily accept the different hydrophobic residues of the other AIPs might result in a more efficient AIP-2 binder. Lastly, a combination of both approaches might yield an AIP-3-specific antibody. Obviously, antibodies with high affinity for two or more different AIP molecules could be useful for passive immunotherapy to prevent or treat infections caused by the different groups of *S. aureus*. AP4-24H11 recognition of the thiolactone ring backbone, which might be a general feature of all staphylococcal AIPs, and the absence of interactions with the N-terminal hydrophobic residues make engineering of AP4-24H11 more feasible. With regard to the use of the AP4 hapten as a scaffold for an active *S. aureus* vaccine, the crystallographic data might be used to delineate a path for further improvement of the AIP haptens to elicit a more AIP cross-reactive immune response. For example, the construction of hybrid macrocyclic AIP haptens incorporating many of the critical features described above, as well an N-terminal tail truncation, might indeed result in a broadly AIP cross-reactive antibody response.

Acknowledgments—We thank Sharon Ferguson for optimizing the IgG digestion conditions, Erik Debler for help with antibody crystallization and diffraction experiments, Jeffrey S. Kavanaugh (University of Iowa) for a critical reading of the manuscript, the Joint Center for Structural Genomics for use of the structure quality control server, and the Advanced Photon Source at Argonne National Laboratory for data collection at beamline 23ID-B.

REFERENCES

1. Fuqua, W. C., Winans, S. C., and Greenberg, E. P. (1994) *J. Bacteriol.* **176,** 269–275
2. Reading, N. C., and Sperandio, V. (2006) *FEMS. Microbiol. Lett.* **254,** 1–11
3. David, M. Z., and Daum, R. S. (2010) *Clin. Microbiol. Rev.* **23,** 616–687
4. Deleo, F. R., Otto, M., Kreiswirth, B. N., and Chambers, H. F. (2010) *Lancet* **375,** 1557–1568
5. Fischbach, M. A., and Walsh, C. T. (2009) *Science* **325,** 1089–1093
6. Clatworthy, A. E., Pierson, E., and Hung, D. T. (2007) *Nat. Chem. Biol.* **3,** 541–548
7. Kaufmann, G. F., Park, J., and Janda, K. D. (2008) *Expert. Opin. Biol. Ther.* **8,** 719–724
8. Projan, S. J., Nesin, M., and Dunman, P. M. (2006) *Curr. Opin. Pharmacol.* **6,** 473–479
9. Suga, H., and Smith, K. M. (2003) *Curr. Opin. Chem. Biol.* **7,** 586–591
10. Lebeau, C., Vandenesch, F., Greenland, T., Novick, R. P., and Etienne, J. (1994) *J. Bacteriol.* **176,** 5534–5536
11. MDowell, P., Affas, Z., Reynolds, C., Holden, M. T., Wood, S. J., Saint, S., Cockayne, A., Hill, P. J., Dodd, C. E., Bycroft, B. W., Chan, W. C., and Williams, P. (2001) *Mol. Microbiol.* **41,** 503–512
12. Recsei, P., Kreiswirth, B., O'Reilly, M., Schlievert, P., Gruss, A., and Novick, R. P. (1986) *Mol. Gen. Genet.* **202,** 58–61
13. Morfeldt, E., Tegmark, K., and Arvidson, S. (1996) *Mol. Microbiol.* **21,** 1227–1237
14. Novick, R. P., Projan, S. J., Kornblum, J., Ross, H. F., Ji, G., Kreiswirth, B., Vandenesch, F., and Moghazeh, S. (1995) *Mol. Gen. Genet.* **248,** 446–458
15. Thoendel, M., and Horswill, A. R. (2009) *J. Biol. Chem.* **284,** 21828–21838
16. Zhang, L., Gray, L., Novick, R. P., and Ji, G. (2002) *J. Biol. Chem.* **277,** 34736–34742
17. Jensen, R. O., Winzer, K., Clarke, S. R., Chan, W. C., and Williams, P. (2008) *J. Mol. Biol.* **381,** 300–309
18. Chen, L. C., Tsou, L. T., and Chen, F. J. (2009) *J. Microbiol.* **47,** 572–581
19. Geisinger, E., George, E. A., Muir, T. W., and Novick, R. P. (2008) *J. Biol. Chem.* **283,** 8930–8938
20. Koenig, R. L., Ray, J. L., Maleki, S. J., Smeltzer, M. S., and Hurlburt, B. K. (2004) *J. Bacteriol.* **186,** 7549–7555
21. Ji, G., Beavis, R., and Novick, R. P. (1997) *Science* **276,** 2027–2030
22. Lyon, G. J., Mayville, P., Muir, T. W., and Novick, R. P. (2000) *Proc. Natl. Acad. Sci. U.S.A.* **97,** 13330–13335
23. Nakayama, J., Uemura, Y., Nishiguchi, K., Yoshimura, N., Igarashi, Y., and Sonomoto, K. (2009) *Antimicrob. Agents Chemother.* **53,** 580–586
24. Park, J., Jagasia, R., Kaufmann, G. F., Mathison, J. C., Ruiz, D. I., Moss, J. A., Meijler, M. M., Ulevitch, R. J., and Janda, K. D. (2007) *Chem. Biol.* **14,** 1119–1127
25. Kaufmann, G. F., Park, J., Mayorov, A. V., Kubitz, D. M., and Janda, K. D. (2011) *Methods Mol. Biol.* **692,** 299–311
26. Marks, J. D., Tristem, M., Karpas, A., and Winter, G. (1991) *Eur. J. Immunol.* **21,** 985–991
27. Harlow, E., and Lane, D. (1988) *Antibodies: A Laboratory Manual*, pp. 626–631, Cold Spring Harbor Laboratory Press, Cold Spring Harbor, New York
28. Otwinoski, Z., and Minor, W. (1997) *Methods Enzymol.* **276,** 307–326
29. McCoy, A. J., Grosse-Kunstleve, R. W., Adams, P. D., Winn, M. D., Storoni, L. C., and Read, R. J. (2007) *J. Appl. Crystallogr.* **40,** 658–674
30. Gruber, K., Zhou, B., Houk, K. N., Lerner, R. A., Shevlin, C. G., and Wilson, I. A. (1999) *Biochemistry* **38,** 7062–7074
31. Emsley, P., and Cowtan, K. (2004) *Acta. Crystallogr. D Biol. Crystallogr.* **60,** 2126–2132
32. Murshudov, G. N., Vagin, A. A., and Dodson, E. J. (1997) *Acta. Crystallogr. D Biol. Crystallogr.* **53,** 240–255
33. Al-Lazikani, B., Lesk, A. M., and Chothia, C. (1997) *J. Mol. Biol.* **273,** 927–948
34. Schüttelkopf, A. W., and van Aalten, D. M. (2004) *Acta. Crystallogr. D Biol. Crystallogr.* **60,** 1355–1363
35. Collaborative Computational Project. (1994) *Acta. Crystallogr. D Biol. Crystallogr.* **50,** 760–763
36. Blanc, E., Roversi, P., Vonrhein, C., Flensburg, C., Lea, S. M., and Bricogne, G. (2004) *Acta. Crystallogr. D Biol. Crystallogr.* **60,** 2210–2221
37. Abhinandan, K. R., and Martin, A. C. (2008) *Mol. Immunol.* **45,** 3832–3839
38. Davis, I. W., Leaver-Fay, A., Chen, V. B., Block, J. N., Kapral, G. J., Wang, X., Murray, L. W., Arendall, W. B., 3rd, Snoeyink, J., Richardson, J. S., and Richardson, D. C. (2007) *Nucleic Acids Res.* **35,** W375–383
39. Sheriff, S., Silverton, E. W., Padlan, E. A., Cohen, G. H., Smith-Gill, S. J., Finzel, B. C., and Davies, D. R. (1987) *Proc. Natl. Acad. Sci. U.S.A.* **84,** 8075–8079
40. Connolly, M. L. (1993) *J. Mol. Graph.* **11,** 139–141
41. McDonald, I. K., and Thornton, J. M. (1994) *J. Mol. Biol.* **238,** 777–793

42. Malone, C. L., Boles, B. R., Lauderdale, K. J., Thoendel, M., Kavanaugh, J. S., and Horswill, A. R. (2009) *J. Microbiol. Methods.* **77,** 251–260
43. Dougherty, D. A. (1996) *Science* **271,** 163–168
44. Gallivan, J. P., and Dougherty, D. A. (1999) *Proc. Natl. Acad. Sci. U.S.A.* **96,** 9459–9464
45. Brandl, M., Weiss, M. S., Jabs, A., Sühnel, J., and Hilgenfeld, R. (2001) *J. Mol. Biol.* **307,** 357–377
46. Burley, S. K., and Petsko, G. A. (1985) *Science* **229,** 23–28
47. Debler, E. W., Kaufmann, G. F., Kirchdoerfer, R. N., Mee, J. M., Janda, K. D., and Wilson, I. A. (2007) *J. Mol. Biol.* **368,** 1392–1402
48. Wright, J. S., 3rd, Lyon, G. J., George, E. A., Muir, T. W., and Novick, R. P. (2004) *Proc. Natl. Acad. Sci. U.S.A.* **101,** 16168–16173
49. Wright, J. S., 3rd, Traber, K. E., Corrigan, R., Benson, S. A., Musser, J. M., and Novick, R. P. (2005) *J. Bacteriol.* **187,** 5585–5594